α-tricalcium phosphate synthesis from amorphous calcium phosphate: structural characterization and hydraulic reactivity

T. Martinez [a], M. Espanol [b], C. Charvillat [c], O. Marsan [c], M.P. Ginebra [b, d], C. Rey [c], S. Sarda [a,*]

[a] CIRIMAT, Université de Toulouse, CNRS, Université Toulouse 3 Paul Sabatier, ENSIACET, 4 allée Emile Monso, 31030 Toulouse cedex 4, France

[b] Biomaterials, Biomechanics and Tissue Engineering Group, Department of Materials Science and Engineering, Universitat Politècnica de Catalunya, Av. Eduard Maristany 10-14, 08019 Barcelona, Spain

[c] CIRIMAT, Université de Toulouse, CNRS, INP ENSIACET, 4 allée Emile Monso, 31030 Toulouse cedex 4, France

[d] Institute for Bioengineering of Catalonia (IBEC), Barcelona Institute of Science and Technology, Baldiri Reixac 10-12, 08028, Barcelona, Spain

[*] Corresponding author:
Stéphanie Sarda,
CIRIMAT, Université de Toulouse, CNRS, INP ENSIACET, 4 allée Emile Monso, 31030 Toulouse cedex 4, France
e-mail: stephanie.sarda@univ-tlse3.fr; Tel: +330 534 323 416

Abstract

In the present study, amorphous tricalcium phosphate (TCP) has been synthetized by a wet route to obtain low temperature α-TCP at 650 °C (LT-αTCP) and compare its structural, physical-chemical and thermal properties with those of α-TCP obtained by the conventional solid-state reaction method at 1400°C (HT-αTCP). Even if no significant differences were observed concerning the values of lattice parameters measured by Rietveld refinement, LT-αTCP presented lower crystallinity and higher crystal strains than HT-αTCP. The reactivity in water of the α-TCP obtained by the two different routes was assessed. Both raw samples appeared relatively inert in solution and did not favour the nucleation of calcium deficient apatite (CDA); the LT-αTCP and HT-αTCP were converted into apatite only after milling. The mechanical process leads to a decrease in crystallinity and the formation of an amorphous phase, which is supported in this work by Raman spectroscopy. The faster rate of conversion of milled LT-αTCP compared to HT-αTCP can be assigned to its higher specific surface area, lower crystallinity and higher residual crystal strain; these favour the dissolution of the α-TCP phase. Finally, the setting properties of α-TCP based bone cements were compared regarding their synthesis route. Although the synthesis route does not significantly affect the setting times, the kinetic of conversion into CDA was faster for LT-αTCP than for HT-αTCP. Thus, the modulation of the dissolution rate of α-TCP based cement determined by the preparation route and the grinding process allows control of the overall setting reaction.

Keywords

Amorphous calcium phosphate; α-Tricalcium phosphate; Rietveld refinements; Calcium phosphate cement; Bone substitute.

1. Introduction

Alpha tricalcium phosphate (α-TCP) is especially interesting as a bioactive material because of its ability to react with water and set at low temperatures to give calcium deficient apatites (CDA) with a composition close to human bone mineral. For these reasons, α-TCP is currently used in several biomaterials such as hydraulic bone cements for filling bone defects [1, 2].

The phase equilibrium diagram of the $CaO-P_2O_5$ system exhibits three polymorphs corresponding to the tricalcium phosphate composition $Ca_3(PO_4)_2$: β-TCP, α-TCP and α'-TCP phases, depending on the temperature [3], (Fig. 1). The α'-TCP phase exists only at temperatures above 1430 °C and, at this time, it does not present any practical interest as it has not been stabilized at room temperature. β-TCP is stable up to 1120 °C with a rhombohedral structure (space group R3c), [4] and, above this temperature, it transforms to monoclinic α-TCP (space group $P2_1/a$), [5]. The synthesis of α-TCP, generally obtained through a phase transition reaction, is rather difficult as this phase, thermodynamically stable only between 1120 and 1470 °C, has to be quenched to avoid the formation of β-TCP impurities [5]. Moreover, due to the sintering and crystal growth occurring at the high temperatures corresponding to the stability domain of the α-TCP phase, it is not possible to obtain particles of α-TCP with a high specific surface area by this conventional and most used preparation route. That reduces the chemical and biological reactivity of the prepared α-TCP phase.

However, α-TCP can also be obtained as a metastable compound by heating amorphous tricalcium phosphate (ATCP), which exhibits the appropriate Ca/P ratio, between 600 and 800 °C, even though the maximum temperature of this formation process is far below the stability domain of α-TCP (Fig. 1), [6]. Above 800 °C, the metastable α-TCP phase, thus obtained is converted into the stable β-TCP one [7-10]. ATCP can be obtained by two main routes: in aqueous medium at low temperature (wet route), [11-13] or by using high energy processing or high temperatures (dry route), [14]. Several authors have reported the synthesis of ATCP by flame spray synthesis [8, 15, 16], but the resulting α-TCP obtained after heating at 600 °C exhibits a lower reactivity than the product classically obtained at high temperature [17].

In the present study, we synthesized ATCP by the wet route developed by Heughebaert et al. [11, 18]. The conversion of ATCP into α-TCP was first shown by Eanes [9] and then studied on thermodynamic basis by Somrani et al. [7]. However, despite the fact that this route entails a significant reduction in the cost of production and opens a rather large low temperature formation domain, limiting grain growth and sintering, the low-temperature α-TCP has been barely exploited to produce cements, contrary to that obtained by the usual high temperature process. Therefore, the objectives of this work were as follows: (i) to compare the structural, physic-chemical and thermal

properties of α-TCP obtained by the two different available routes (by conventional solid state reaction at 1400 °C and from ATCP conversion at 650 °C) and (ii) to examine the effect of the synthesis route on the hydraulic conversion of the α-TCP into apatite and the reactivity, setting and final properties of the cements in view of bone filling applications.

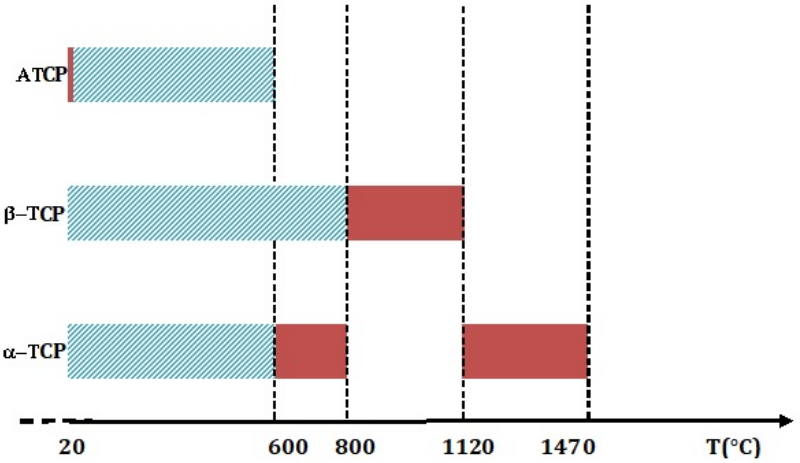

Figure 1. *Domain of formation (dark red) and existence (light blue) of amorphous calcium phosphate (ATCP), β-tricalcium phosphate (β-TCP) and α-tricalcium phosphate (α-TCP), (inspired from [10]).*

2. Materials and Methods

2.1 *Powders synthesis*

Amorphous tri-calcium phosphate (ATCP, Ca/P=1.5) was synthesized by double decomposition of calcium and phosphate salts dissolved in aqueous solutions at room temperature and pH close to 10 [7, 11, 14, 18]. A calcium nitrate solution, $Ca(NO_3)_2{\cdot}4H_2O$ (43.6 g in 550 mL of water containing 40 mL of NH_4OH 30%),was mixed quickly with a phosphate-containing solution, $(NH_4)_2HPO_4$ (27.3 g in 1300 mL of water containing 40 mL of NH_4OH 30%). After filtration, the precipitate was washed and lyophilized during 48 h.

Two α-TCP synthesis routes have been studied: (i) a low temperature route (named LT-αTCP) using thermal treatment of the ATCP obtained by wet double decomposition method at 650 °C for 30 min; (ii) a high temperature dry route (named HT-αTCP) using a solid state reaction at 1400 °C (based on a referenced method) by mixing calcium hydrogen phosphate $CaHPO_4$ and calcium carbonate $CaCO_3$ [1]. The sintered raw HT-αTCP was lightly ground manually in an agate mortar. α-TCP powders were milled using a Pulverisette 6 (Fritsch GmbH): 35.5 g α-TCP powder was processed in a 10 cm diameter agate bowl (6 agate beads, Ø = 3 cm,) at 450 rpm for 15 min.

2.2 Solid samples characterization

X-ray diffraction (XRD) analysis was carried on a BRUKER D8 Advance diffractometer (CuKα radiation, 40 mA, 40 kV). The 2θ range was 10°- 80° (step size of 0.01°, time/step of 1s). The α-TCP lattice parameters were determined by least square Rietveld refinement from the well-determined positions of the most intense reflections using the Thompson-Cox-Hastings pseudo-Voigt peak shape function (Fullprof program). Apparent sizes (d) were calculated using Scherrer Formula [19]. Max strains (in %%) correspond to 1/4 of the apparent strain defined by Stokes and Wilson (Eq. 1), [20]:

$$\text{Strain} = e = 1/2 * \beta * d \qquad \text{(Eq.1)}$$

with β being the integral breadths given in reciprocal lattice units (1/Å) x 1000.

The specific surface area was measured by nitrogen adsorption (Brunauer-Emmett-Teller method) using ASAP 2020 equipment (Micromeritics). Before measurement the powder was outgassed at 100 °C.

Raman analyses were carried out using a confocal Raman microscope Horiba Labram HR 800 Jobin Yvon. The samples were exposed to a continuous laser radiation provided by an Argon diode laser at 532 nm (8 mW). A macrospot module was used to obtain a spot size of 100x100 µm. Raman spectra were acquired through a grating of 1800 lines per mm (spectral resolution of 1 cm^{-1}) with a quantum well detector cooled to - 60 ° C (Synapse CCD). Each spectrum was recorded between 900-1100 cm^{-1} (integration time of 240 s, 3 accumulations). A certified silicon standard allowed frequency equipment to be calibrated using the silicon line at 520.7 cm^{-1}. A baseline correction and fitting processing were realized using Labspec 5 software (Horiba Jobin Yvon) by varying parameters (position and width of phosphate bands) to provide the best curve fit. The baseline was linearized, and the band shape was considered to be Gaussian-Lorentzian.

Differential thermal analysis (DTA) of ATCP and α-TCP was performed using a SetSys Evolution 1600 SETARAM apparatus with a heating rate equal to 10°C/min.

Hydraulic reactivity profiles consist of an evaluation of α-TCP reactivity and transformation ability using only pH variations in solution. To preserve of the sensitivity of this technique no buffer can be used. These profiles were obtained at constant temperature in a regulated bath (37 ± 1 °C) with external circulation connected to a double wall cell. The experiments were carried out in triplicate by dispersing α-TCP powders (25 mg) in deionized water (20 mL) with a liquid-to-powder ratio (L/S) equal to 80 mL/g under stirring. The pH, temperature and conductivity were measured every 20 sec. The powders were added to water approximately 2 min after the start of the measurements, removed by filtration of the solution at 8, 15, 18, 24, 30 h, quenched in acetone to stop the reaction, and dried.

2.3 Setting properties of the cement

The cement samples were obtained by mixing α-TCP powders with an aqueous solution containing 2.5 wt % of disodium hydrogenphosphate as an accelerant with an L/P ratio equal to 0.45 mL/g. The initial (I) and final (F) setting times, determined with Gillmore needles (ASTM-C266-89 standard method), are defined as the time a small needle (113.4 g, Ø=2.13 mm, 0.3 MPa) and a large needle (453.6 g, Ø=1.06 mm, 5 MPa) no longer leave a visible print on the surface of the cement paste. The cement pastes were placed in Teflon moulds (Ø = 6 mm, h = 12 mm) and immersed in Ringer's solution at 37°C. The samples were removed from their moulds at 0, 18, 24, 48, 168 h, and dropped in acetone to stop the setting reaction, dried, ground to powder, and characterized by XRD. The apparent crystallite size was calculated from the (002) lines by applying Scherrer's formula [19]. The relative intensity for each component was calculated by indexing the peaks using JCPDS-9-348 for α-TCP and JCPDS-9-432 for CDA. The compressive strength was measured using a mechanical testing machine (HOUNSFIELD H25KS Model, 25kN) with a crosshead speed of 1 mm/min. Scanning electron microscopy (SEM) observations were performed using an FEG JEOL JSM 6700F.

3. Results

3.1 Characterization of the powders

3.1.1 Thermal evolution of ATCP into LT-αTCP

The X-ray diffraction diagram of the ATCP powder (Fig. SI1) shows the characteristic features of an amorphous compound with broad humps around 30° and 50° and no additional peak of a crystalline phase. Moreover, after heating the sample at 900 °C for 2 h, no apatite was observed by XRD and no pyrophosphate groups by FTIR spectroscopy (data not shown). According to Heughebaert [21], this is indicative of pure amorphous tricalcium phosphate (Ca/P=1.5, above 98%).

The DTA curve of ATCP powders from 25 to 1200 °C (Fig. SI2) shows an asymmetric endothermic peak with a minimum at about 190 °C that is associated with water loss and an intense exothermic peak at about 680 °C which was attributed by Somrani et al. [7] to the crystallization of the amorphous phase.

The structural evolution of ATCP was characterized by XRD after heating 1g of the amorphous powder in an oven at different constant temperatures from 25 to 850 °C for 30 min (Fig. 2). Considering the phase diagram of the P_2O_5-CaO system [3], β-TCP is normally thermally stable up to its phase transition into α-TCP at a temperature of 1120 °C, then α-TCP is stable between 1120 and 1470 °C but metastable at room temperature [2]. According to Fig. 2, ATCP remained amorphous until 550 °C, and its crystallization into α-TCP occured between 550 and 650 °C; this was at a lower temperature than the crystallization peak observed on the thermal analysis, a difference usually

observed between dynamic and static heating modes. Then the metastable α-TCP begins to re-crystallise into stable β-TCP, and the α and β phases coexist between 750 and 850°C. Thus, the thermodynamically unstable phase at these temperatures forms first, which is in agreement with the Ostwald step rule [22].

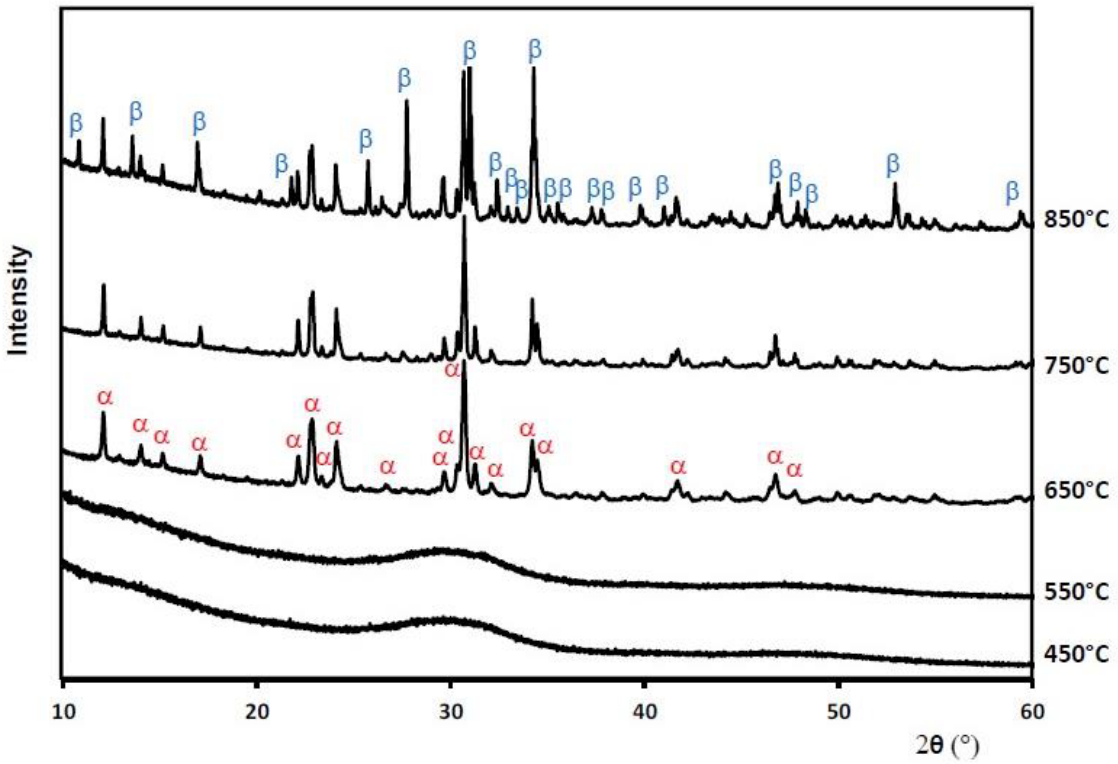

Figure 2. *XRD diffraction of ATCP after heating in a range of temperature between 450 and 850 °C (α and β for α-TCP and β-TCP main XRD peaks, respectively).*

3.1.2 Structural properties of α-TCP

3.1.2.1 Influence of synthesis route

SEM observations of α-TCP powders produced at low and high temperature after 15 min of milling are presented in Fig. 3. Particle agglomerates with a dimension of few µm are observed for both powders. HT-αTCP appears compact due to the high temperature process, whereas LT-αTCP appears as looser agglomerates. Specific surface area values are about 5 times lower for α-TCP obtained by conventional synthesis: 2.0 ± 0.2 and 11 ± 1 and m^2/g for HT-αTCP and LT-αTCP, respectively. It can be noted that the results of specific surface area for HT-αTCP are in accordance with those published in the literature [23-26].

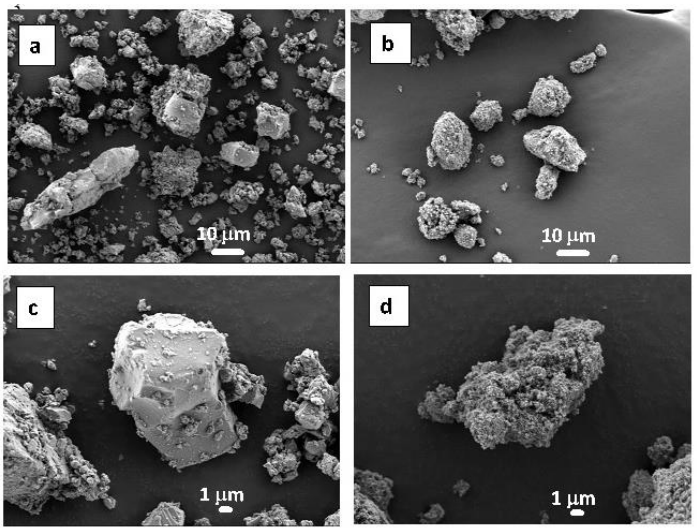

Figure 3. *SEM observations of α-TCP powders milled 15 min (a), (c) HT-αTCP; (b), (d) LT-αTCP.*

XRD diagrams of the two α-TCP powders milled for 15 min (Fig. 4) show pure α-TCP phase with no additional peak. However, the LT-αTCP diagram presents lower intensity and broader peaks, suggesting a lower crystallinity than that of the HT-αTCP sample. The crystalline structure of α-TCP was first published by Mackay et al. in 1953 [27], then studied by Mathew et al. in 1977 [5, 27] and more recently by Yashima et al. [23, 28]. Structural Rietveld refinements from XRD data of LT-αTCP and HT-αTCP were successfully performed in the monoclinic system $P2_1/a$ (Fig. 4). The lattice parameters, apparent crystal size and maximal strain calculated by Rietveld refinement are presented in Table 1 [5, 23, 28]. The structural parameters obtained agreed with those published (Table 2) but significant differences were observed concerning the apparent crystal size and strain depending on the synthesis route and mechanical treatment. LT-αTCP powder presents a smaller apparent crystal size (about 675 ± 30 and 3585 ± 500 Å for unmilled LT-αTCP and HT-αTCP, respectively), lower crystallinity and higher maximum strain than HT-αTCP.

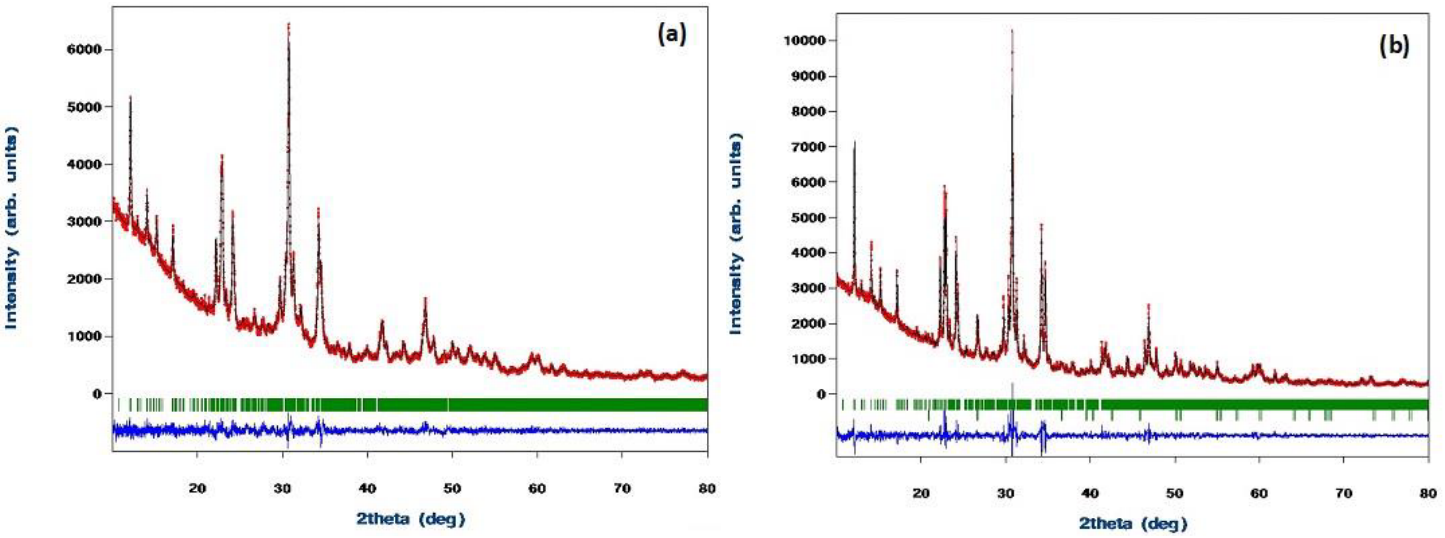

Figure 4. *XRD diagrams and Rietveld refinement of milled (15 min) α-TCP: (a) LT-αTCP) and (b) HT-αTCP. The black lines (Y_{calc}) are calculated intensities and the red points (Y_{obs}) the observed intensities. The difference between the observed and calculated intensities (Y_{obs}-Y_{calc}) is plotted in blue line below the profile. The short vertical green lines show the position of Bragg reflections.*

Table 1. *Lattice parameters, apparent crystal size and maximal strain obtained by Rietveld refinement from XRD data of α-TCP powders, as synthesized (LT-αTCP and HT-αTCP) and milled.*

α-TCP powder	Milling time	a (Å)	b (Å)	c (Å)	β (°)	App-size (Å)	Max-strain (%%)
LT-αTCP	0 min	12.8598(2)	27.2241(2)	15.1863(1)	126.201(1)	675 ± 30	10.5 ± 0.8
	15 min	12.8740(3)	27.2808(3)	15.2098(2)	126.220(2)	842 ± 30	20 ± 2
HT-αTCP	0 min	12.84247(8)	27.33254(9)	15.21115(5)	126.3083(5)	3585 ± 500	2.7 ± 0.7
	15 min	12.8414(2)	27.3274(2)	15.2087(2)	126.3086(1)	1905 ± 60	9.0 ± 0.3

Table 2. *Structural data of α-TCP reported in the literature obtained by Rietveld refinement from X-ray or neutron diffraction data [5, 23, 28]. All the values were determined on α-TCP obtained by solid state reaction at 1400 °C.*

Reference	a (Å)	b (Å)	c (Å)	β(°)
Mathew et al. [5]	12.887(2)	27.280(4)	15.219(2)	126.20(1)
Yashima and Sakai [28]	12.859(2)	27.354(2)	15.222(2)	126.35(1)
Yashima et al. [23]	12.87271(9)	27.28034(8)	15.21275(12)	126.2078(4)

3.1.2.2 Influence of mechanical treatment

3.1.2.2.1 Structural analysis

Figure 5 shows XRD diagrams of the LT-αTCP phase obtained from ATCP powder at 650 °C, unmilled and after 15 min of ball milling time. Milling leads to broad XRD peaks with low intensity. In addition, the broad hump around 30° in milled samples can be related to an amorphization of the α-TCP phase due to milling, in agreement with data already reported [25, 29].

The two types of α-TCP studied in this work exhibit similar lattice dimensions, and the milling process does not have any significant consequences on these values (Table 1). Moreover, the crystal size calculated for HT-αTCP powder decreases strongly after 15 min of milling (from 359 nm ± 50 to 191 nm ± 6), while this value appears slightly larger for LT-αTCP after 15 min of milling (from 68 nm ± 3 to 84 nm ± 3). This can be due to a bias in the determination of the average size excluding the amorphized part of the sample and the smaller crystals participating only to the base enlargement of the diffraction lines excluded by the background corrections. Moreover, a significant increase of maximum crystal strain parameter was observed after 15 min of milling, whatever the synthesis route.

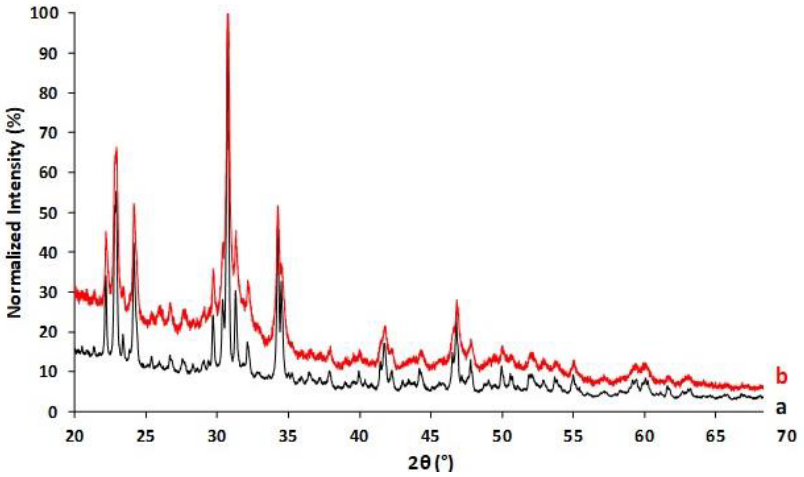

Figure 5. *XRD diagrams of: (a) unmilled and (b) milled (15 min) LT-αTCP. The Y axis corresponds to the standardized intensity relative to maximum intensity (normalized intensity in %).*

3.1.2.2.2 Thermal evolution

The DTA curves from 250 to 650 °C for the LT-αTCP and HT-αTCP powders before and after milling are presented in Fig. 6. A broad exothermic peak was observed at about 530 °C after 15 min of milling whatever the synthesis route. This peak could be associated to the crystallization of an amorphous phase related to grinding because it is not observed in the unmilled samples; such a recrystallization phenomenon after milling has also been reported by Camiré et al. [25] for milled HT-αTCP at slightly lower temperatures (400-450 °C).

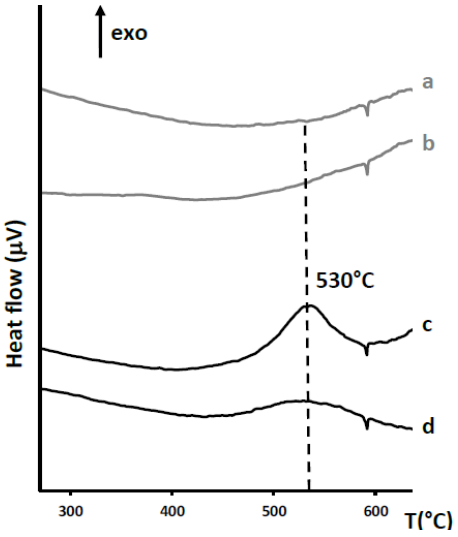

***Figure 6**. DTA curve of unmilled (a) HT-αTCP, (b) LT-αTCP; and of milled (c) HT-αTCP, (d) LT-αTCP.*

3.1.2.2.3 Raman investigations

Raman spectra of LT-αTCP et HT-αTCP with and without milling (15 min) are presented in Fig. 7. Factor group analysis predict that the primitive cell of α-TCP should exhibit 216 Raman bands for internal modes of the PO_4^{3-} ion [30], but fewer vibration bands than predicted are observed in Raman spectra. The most prominent bands of α-TCP are present between 900-1000 cm^{-1}, as published by previous authors [31]. There are attributed to the ν_1 symmetric P-O stretching vibration of the phosphate ion. The presence of a medium intensity line at 984 cm^{-1} has been assigned to the ν_3 fundamental vibrational mode corresponding to the triple-degenerate asymmetric P-O stretching mode [30]; other bands corresponding to this mode are found at 998, 1012, 1027, 1058 and 1077 cm^{-1}.

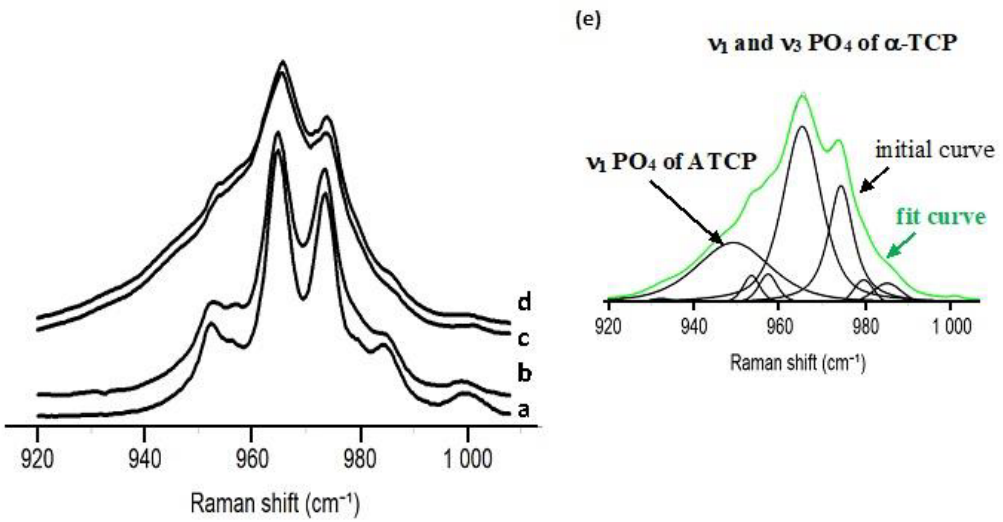

***Figure 7.** Raman spectra of (a) unmilled and (c) milled HT-αTCP, (b) unmilled and (d) milled LT-αTCP; (e) Decomposition of Raman spectrum of milled LT-αTCP in the domain of 900-1000 cm^{-1}.*

The most obvious difference between milled and unmilled samples is line broadening and the existence of a prominent broad band on the low wavenumber side of the ν_1 PO_4 vibrational domains. This broad line centred at 951 cm^{-1} is related to the milling process, whatever the synthesis route, and it can be assigned to the ν_1 PO_4 line of an amorphous phase [31, 32]. To evaluate the proportion of this phase, a curve fitting was performed, and the relative band integrated intensities were defined as the ratio of ν_1 PO_4 vibration band area of ATCP to the total area of PO_4 bands in the 900-1000 cm^{-1} range. This value was close to zero for unmilled α-TCP, and it increased considerably after 15 min of milling (above 0.3) for both HT-αTCP and LT-αTCP. These results provide evidence for the formation of an amorphous calcium phosphate phase with rather similar amounts in the milled samples whatever the synthesis route.

3.1.2 Reactivity of α-TCP powders

Reactivity assessment of α-TCP powders was performed at 37 °C in deionized water by pH measurements during about 20 h (Fig. 8). The hydrolysis reaction was stopped after 8, 15, 18, 24, 30 h by immersion in ethanol, and the powders were characterized by XRD analysis (Fig. 9). In all cases the first event detected is powder dissolution associated with an uptake of protons and a sharp pH increase that is due to the hydrolysis of dissolved PO_4^{3-} ions into HPO_4^{2-} and $H_2PO_4^-$ ions.

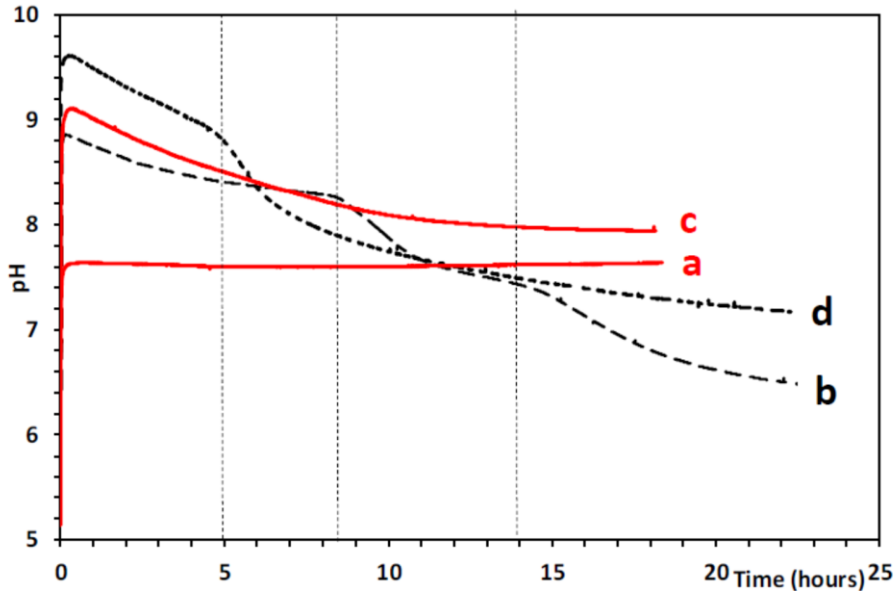

Figure 8. *Kinetics of pH of α-TCP powders suspensions (L/S = 80 mL/g, 37 °C): (a) LT-αTCP without milling; (b) milled LT-αTCP; (c) HT-αTCP without milling and (d) milled HT-αTCP.*

Without ball milling, no transformation into CDA was detected by XRD during the test period whatever the synthesis route (Figure SI3). As seen in Figs. 8a and 8c, after a sharp pH increase related

to the powder dissolution, the values remain stable and neutral (7.6 for LT-αTCP and 8 for HT-αTCP). There is no significant pH decrease, which in agreement with the extremely low rate of hydrolysis reported for unmilled α-TCP first by Monma and Kanazawa [33].

For milled powders, after the initial pH increase related to the dissolution of α-TCP, the pH kinetics exhibited several decrease events that are related to the transformation of the α-TCP into CDA (Fig. 9). The addition of HT-αTCP to water led to a rapid increase of the pH value, which reaches a maximum of 9.6 in few sec before decreasing continuously during the test. The rate of decrease is not constant, and it can be divided into several regions; after about 5 h, a rapid pH decrease is followed by a slower decrease. The XRD study of the powders shows that CDA becomes detectable at only 18 h of HT-αTCP hydrolysis, and no α-TCP phase is detected at 30 h (Fig. 9). Comparatively, mixing LT-αTCP with water leads to a rapid increase in pH up to 8.8 in few sec before decreasing. As with HT-αTCP, the rate of decrease can be divided in several steps showing two fast decrease periods at 8.5 and 14 h. The pH reaches lower values (pH 6.4) than those of HT-αTCP at the end of the test. The XRD diagrams of the powders show that the observation of CDA is delayed. At 8 h no CDA is observed, and a small amount is seen at 15 h. These data indicate that the formation of CDA occurs only after an important lag time, but once this phase has nucleated, the hydrolysis reaction is completed in a few hours and, only CDA is observed at 24 h (Fig. 9). Nevertheless, the transformation reaction of α-TCP into CDA appears globally faster for LT-αTCP. This observation can be related to the higher specific area and the lower crystallinity of LT-αTCP compared to HT-αTCP. Additionally, the XRD peaks of the CDA formed appear less resolved for LT-α-TCP, suggesting the formation of an apatitic phase with a lower crystallinity.

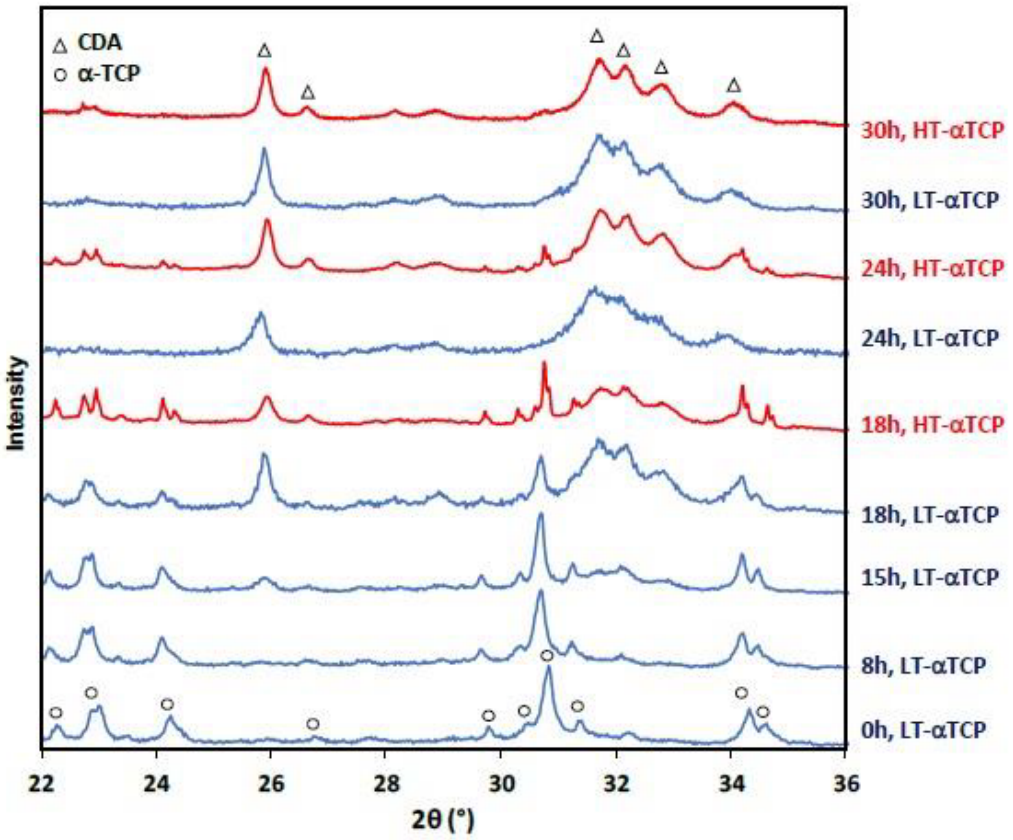

Figure 9. XRD diagrams of milled α-TCP obtained by the two different routes (LT-αTCP *in blue*; HT-αTCP *in red*) hydrolyzed for increasing time periods (L/S = 80 mL/g, 37 °C).

3.2 Bone cement applications

3.2.1 *Setting properties*

Setting properties of the α-TCP based cements obtained by the two different routes and milled for 15 min were studied with a L/S equal to 0.45 mL/g and 2.5 wt.% Na_2HPO_4 as accelerant in the liquid phase. These experimental conditions are clearly different from those used in the previous paragraph but correspond closely to those of α-TCP cement [34]. The initial and final setting times of the cement formulated with LT-αTCP were similar to those obtained with HT-αTCP: I was equal to 24 ± 2 min and 22 ± 1 min for LT-αTCP and HT-αTCP, respectively; F was 75 ± 5 min for both. Whereas the reaction transformation of α-TCP into CDA was not achieved before 48 h for HT-αTCP, as seen in Fig. 10a and Table 3, full conversion was reached in less than 24 h for LT-αTCP (Fig. 10b). These results are in agreement with the hydrolysis data (see 3.1.2) despite the rather different reaction conditions. The crystal size of the CDA formed seems slightly smaller for LT-αTCP than HT-αTCP. As usually observed [34, 35], there is no clear correlation between the setting times determined by the Gillmore needles and the advancement of the hydrolysis reaction determined by XRD.

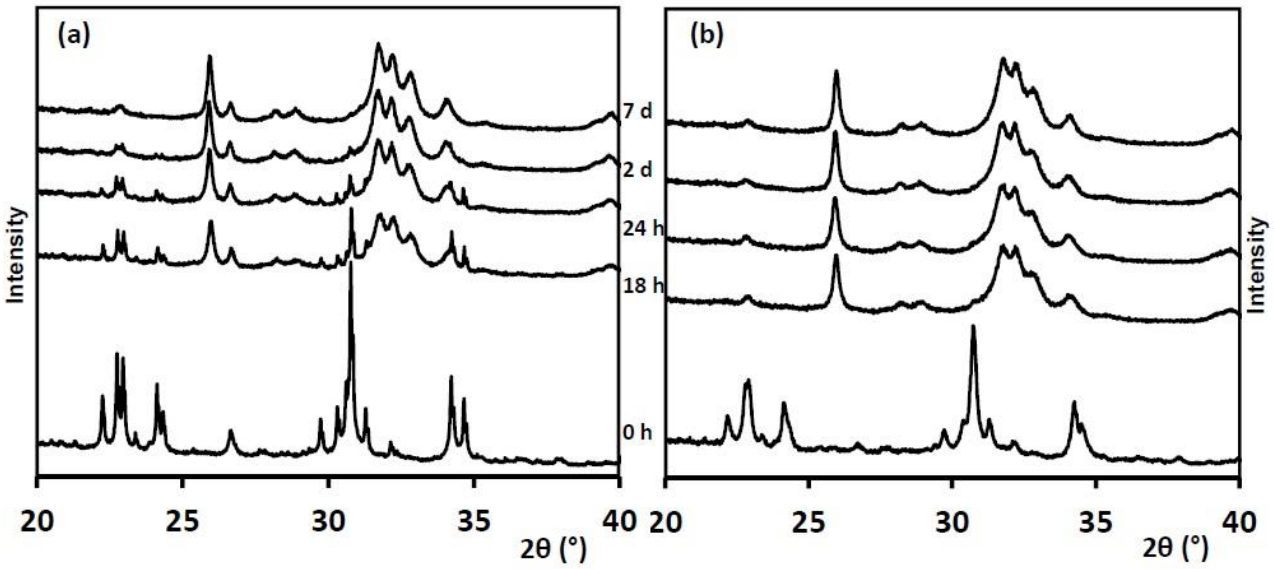

Figure 10. *XRD diagrams of cement obtained with (a) HT-αTCP and (b) LT-αTCP powders at different hardening times in Ringer's solution (L/S = 0.45 mL/g, 2.5 wt.% Na_2HPO_4).*

Table 3. *Weight percent of conversion of LT-αTCP and HT-αTCP based cements into CDA and L(002) apparent crystallite size calculated from the (002) XRD lines of CDA obtained at different hardening times.*

Hardening time	HT-αTCP cement		LT-αTCP cement	
	L(002) ± 30 Å	wt.% CDA	L(002) ± 30 Å	wt.% CDA
18 hours	540	79	420	95
1 day	580	87	370	96
2 days	520	94	460	97
7 days	610	96	410	98

3.2.2 *Compressive strength*

The final compressive strengths (C_s) of cement cylinders after immersion in Ringer's solution for 18, 24, 40 h, and 7 days are presented in Fig. 11a. C_s increased until 24 h for both cements and then remained stable after 48 h. The best values obtained for both cements were around 10-15 MPa. These values are significantly higher for the cement formulated from HT-αTCP. This is in accordance with crystal size (Table 3), and previous work has shown that the evolution of the growth of the apatitic crystals is responsible for the mechanical properties [36]. However, no difference in size and morphology of CDA crystals was detected by SEM up to 48 h (Fig. 11).

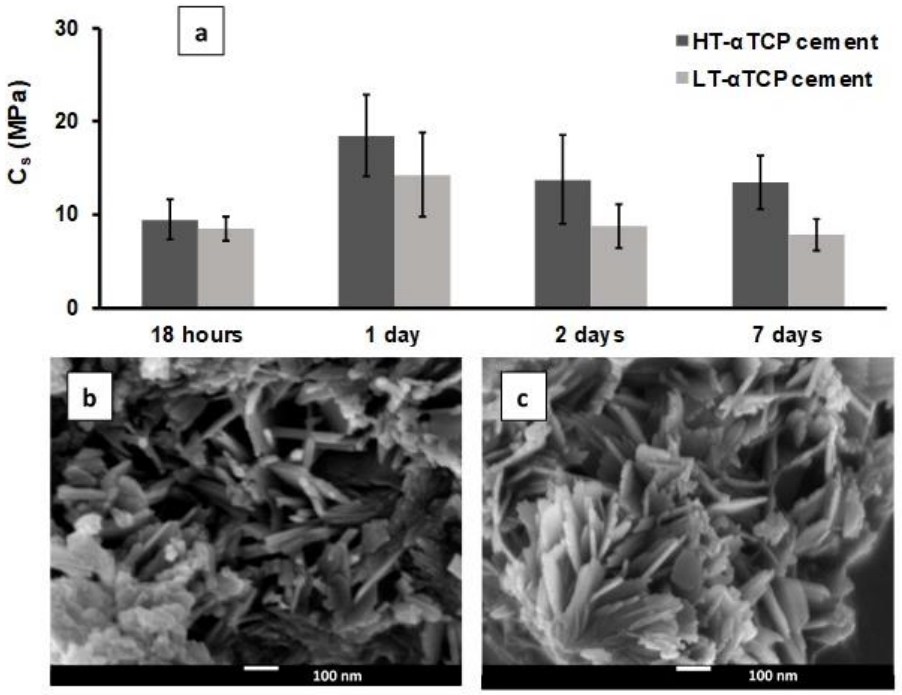

Figure 11. *(a) Compressive strength (C_s) of cement formulated from LT-αTCP and HT-αTCP at different hardening times in Ringer's solution (L/S = 0.45 mL/g, 2.5 wt.% Na_2HPO_4); SEM observations of cement formulated from (b) HT-αTCP and (c) LT-αTCP after 48 h of hardening.*

4. Discussion

The setting reaction and the role of grinding in α-TCP based cements have been the object of several studies [2, 25, 37, 38]. Several articles have pointed out a loss of crystallinity and the formation of an amorphous phase on grinding [25, 39] that is associated with an increase in the conversion reaction rate [39]. Isothermal calorimetry following the hydrolysis reaction suggests that two heat releases occur at different setting times in mixed amorphous-αTCP obtained by milling (200-300s and 5000s), [25]. The study of the setting reaction of α-TCP obtained by thermal conversion of an amorphous calcium phosphate produced by flame spray synthesis revealed a slower rate of conversion that mainly resulted in an increase of the induction time [17]. Generally, the induction time corresponds to the time needed for the first nuclei of CDA to form. In the case of heterogeneous nucleation, it is related to the interfacial tension between the nucleating substrate and the forming nucleus [40, 41].

In the present study, XRD analysis of ATCP at different heating temperatures (Fig. 2) show that thermodynamically unstable α-TCP occurs first between 550 and 650 °C and it recrystallizes into stable β-TCP between 750 and 850 °C, in accordance with previous studies [2, 7]. The formation of crystalline metastable phases during heating of amorphous compounds has been explained by the Ostwald's step rules or the law of successive reactions [22]. It states that in metastable systems, the

closer phase in terms of free energy often crystallizes first, followed by solid state transitions to thermodynamically more stable phases. Even if no significant differences were observed concerning the values of lattice parameters measured by Rietveld refinement, LT-αTCP presents lower crystallinity and higher maximal crystal strains than HT-αTCP. The conventional high temperature process of α-TCP synthesis favours crystal growth and the relatively low temperature involved in the conversion of ATCP to LT-αTCP implies lower ion mobility, preserving smaller particles. However, the high temperatures also favour the formation of thermal defects which might be preserved in the final HT-αTCP due to the quenching.

The ball milling process leads to a decrease in crystallinity and the formation of an amorphous phase (mATCP) as evidenced by DTA, Raman spectroscopy and, with lower sensitivity, by XRD. Thus the starting material is converted into a biphasic powder. Without affecting lattice parameters, ball milling of the powders for only 15 min also involves a significant increase in the maximum crystal strain, creating high energy fracture faces with a high reactivity that determine the behaviour of the powder in solution. The events occurring when α-TCP is dipped in water were investigated in relation to the synthesis method using a simple pH follow-up (Fig. 8). The main events are a dissolution reaction associated with an initial sharp pH increase, the possible re-equilibration of the solutions due to milling, and the CDA nucleation and growth.

The initial pH increase corresponds to the dissolution of the powders, more precisely, it is related to the amount of phosphate ions dissolved. The difference in the amount dissolved between the non-milled LT-αTCP and HT-αTCP is revealed by the maximum value reached by the pH. This could be due to thermodynamic reasons and/or to differences in surface-solution reactions. Such differences in dissolution have already been reported by Bohner et al. [41] between raw α-TCP and α-TCP reheated at 500 °C, using isothermal calorimetry, and the difference in solubility was assigned to dissolution inhibition. Such inhibition of dissolution reactions in under-saturated media has been described and by Tang and Nancollas for octacalcium phosphate and other sparingly soluble salts, and attributed to the lack of active surface defects on the crystals faces [42]. The absence of surface defects in the unmilled LT-αTCP would thus lead to a pseudo-equilibrium of solubility lower than that reached by HT-αTCP. Another possible explanation would be the difference in the dissolution enthalpy of LT-αTCP and HT-αTCP determined by Somrani et al. [7], (-536.3±1.5 and -512.4±1.8 J/g, respectively), indicating that LT-αTCP is more stable regarding dissolution.

Without milling, the α-TCP phases (LT and HT) do not transform into CDA (at least during 20 h, Fig. SI3). This observation is in agreement with the data initially reported by Monma et al. [43, 44].

After the first short period of dissolution (a few min), the pH remains quasi-stable for the non-milled LT-αTCP; for non-milled HT-αTCP, a slow very small decrease is observed during the 20 h of the experiment. This phenomenon reveals the absence of spontaneous nucleation sites for CDA on unmilled α-TCP as there is for β-TCP [45, 46], which implies the need for a higher supersaturation regarding CDA nuclei formation and the start-up of hydrolysis.

Whatever the synthesis route, this lack of reactivity is swept out after milling. For both milled samples the initial increase of pH is higher than that observed for the raw powders, confirming that mechanical grinding favours sample dissolution overpassing the solubility products. Moreover, the milling decreases the crystallinity of α-TCP whatever the synthesis route, and involves the formation of a potentially more soluble amorphous phase (mATCP). The higher dissolved amounts of milled α-TCPs, compared to unmilled ones, do not however allow CDA nucleation according to XRD. The very slow pH decrease which follows the dissolution is similar to that obtained for unmilled α-TCP. This can be assigned to surface re-equilibration of particles with solution. However, the fast pH decreases of the two samples at about 5 and 8.5 h for HT-αTCP and LT-αTCP, respectively (Fig. 8), testify to a nucleation of a Ca-P phase with a lower solubility product than the initial phases. For both LT- and HT-αTCP, a small CDA amount is clearly observed on XRD diagrams at 15 and 18 h, respectively (Fig. 9); it cannot be excluded that an amorphous Ca-P hydrated phase forms first from the hydrolysis of α-TCP or mATCP both present in these biphasic powders. Such a neo-formed amorphous precursor could be a necessity due to the difficulty to nucleate CDA on the α-TCP and the requirement of high supersaturation [47]. Precipitated ATCP can hydrolyze easily into CDA through an autocatalytic hydrolysis reaction as shown by Eanes [9]. The difference in induction times between the milled HT-αTCP (5 h) and LT-αTCP (8.5 h) can be related to the higher supersaturation reached in the HT-αTCP solution, as it is well established that induction times for nucleation decrease as the supersaturation increases. The slowdown in the pH after this first fast pH decrease indicates the installation of the dissolution-reprecipitation process at a lesser ion activity product in solution. A second fast decrease with the milled LT-αTCP occurs at around 14 h, corresponding to CDA detection by XRD with a second adjustment to a new inferior ionic product of solution. The HT-αTCP curve shows only one major event in solution, possibly because the formation of apatite appears slower. These two conversion steps, clearly observed in the pH variation/evolution for LT-αTCP, have also been observed by Camire et al. in α-TCP cements using isothermal calorimetry, although at much earlier times [25]. Once apatite nucleation has occurred, the dissolution-reprecipitation reaction is active and it is the dissolution rate of the initial α-TCP phases, related to their specific surface area, which is the limiting factor of the conversion reaction into CDA. Another fact to consider

regarding the hydrolysis rate is that LT-αTCP induces a larger pH drop and thus facilitates the dissolution process; this could be related to differences in the composition of formed CDAs depending on the initial powder which have to be analyzed, but essentially to the higher specific surface area of LT-αTCP which makes it more reactive.

Regarding the trials on α-TCP based cements, the synthesis route of the initial powders does not significantly affect the setting times. The C_s values remained low (around a maximum of 10-15 MPa) but suitable for filling non-load-bearing bone defects. However, XRD data show that LT-αTCP presents faster conversion kinetics into CDA than HT-αTCP. This is in agreement with the reactivity study of the powders in water which was performed at a much higher L/S ratio (80 instead of 0.45 mL/g in setting experiments) and in different conditions (Na_2HPO_4 as accelerator in the cement). The reaction rate seems to be mainly controlled by the dissolution rate of the α-TCP/mATCP biphasic sample, once the nucleation of CDA has occurred, with induction periods similar to those observed in the testing of the powders' reactivity. Thus the preparation route and grinding allows the control of the overall setting reaction. Although the powder reactivity assessment was performed at high L/S, they appear nicely related to the cements conversion reaction including the induction time. Therefore, simple tests such as monitoring the pH evolution could be used to understand the behaviour of cement mixtures.

5. Conclusion

In the present study, it appears that the milling process acts on the α-TCP reactivity. It not only favours the dissolution rate of the powder through increased surface area but also the formation of an amorphous phase and surface instabilities. The synthesis route acts on the structure stability of α-TCP based cement by modifying the rate of CDA nucleation.

Acknowledgements

M.P.G. acknowledges the support provided by the Spanish Government through Project MAT2015-65601-R (MINECO/FEDER, UE), and the "Generalitat de Catalunya" for the 2017 SGR11-65 and the Icrea Academia Award. M.E. acknowledges the Serra Hunter Fellowship. This project was supported by Inca-Cancéropôle GSO under the DOXOSARCOME project.

Conflict of interest

The authors declare that they have no conflict of interests in this paper.

References

[1] M.-P. Ginebra, M. Espanol, E.B. Montufar, R.A. Perez, G. Mestres, New processing approaches in calcium phosphate cements and their applications in regenerative medicine, Acta Biomaterialia 6(8) (2010) 2863-2873.

[2] R.G. Carrodeguas, S. De Aza, α-Tricalcium phosphate: Synthesis, properties and biomedical applications, Acta Biomaterialia 7(10) (2011) 3536-3546.

[3] J.C. Elliott, Structure and chemistry of the apatites and other calcium orthophosphates, Elsevier Amsterdam ed.1994.

[4] B. Dickens, L. Schroeder, W. Brown, Crystallographic studies of the role of Mg as a stabilizing impurity in β-$Ca_3(PO_4)_2$. The crystal structure of pure β-$Ca_3(PO_4)_2$, Journal of Solid State Chemistry 10(3) (1974) 232-248.

[5] M. Mathew, L. Schroeder, B. Dickens, W. Brown, The crystal structure of α-$Ca_3(PO_4)_2$, Acta Crystallographica Section B 33(5) (1977) 1325-1333.

[6] T. Kanazawa, T. Umegaki, N. Uchiyama, Thermal crystallisation of amorphous calcium phosphate to α-tricalcium phosphate, Journal of chemical Technology and Biotechnology 32(2) (1982) 399-406.

[7] S. Somrani, C. Rey, M. Jemal, Thermal evolution of amorphous tricalcium phosphate, Journal of Materials Chemistry 13(4) (2003) 888-892.

[8] M. Maciejewski, T.J. Brunner, S.F. Loher, W.J. Stark, A. Baiker, Phase transitions in amorphous calcium phosphates with different Ca/P ratios, Thermochimica Acta 468(1-2) (2008) 75-80.

[9] E. Eanes, Thermochemical studies on amorphous calcium phosphate, Calcified Tissue Research 5(1) (1970) 133-145.

[10] C. Rey, C. Combes, C. Drouet, S. Somrani, 15 - Tricalcium phosphate-based ceramics, in: T. Kokubo (Ed.), Bioceramics and their Clinical Applications, Woodhead Publishing 2008, pp. 326-366.

[11] J.-C. Heughebaert, G. Montel, Conversion of amorphous tricalcium phosphate into apatitic tricalcium phosphate, Calcified Tissue International 34 (1982) S103-8.

[12] S. Somrani, M. Banu, M. Jemal, C. Rey, Physico-chemical and thermochemical studies of the hydrolytic conversion of amorphous tricalcium phosphate into apatite, Journal of Solid State Chemistry 178(5) (2005) 1337-1348.

[13] A. Rodrigues, A. Lebugle, Influence of ethanol in the precipitation medium on the composition, structure and reactivity of tricalcium phosphate, Colloid Surf. A-Physicochem. Eng. Asp. 145(1-3) (1998) 191-204.

[14] C. Combes, C. Rey, Amorphous calcium phosphates: synthesis, properties and uses in biomaterials, Acta Biomaterialia 6(9) (2010) 3362-3378.

[15] N. Döbelin, T.J. Brunner, W.J. Stark, M. Fisch, E. Conforto, M. Bohner, Thermal Treatment of Flame-Synthesized Amorphous Tricalcium Phosphate Nanoparticles, Journal of the American Ceramic Society 93(10) (2010) 3455-3463.

[16] S. Loher, W.J. Stark, M. Maciejewski, A. Baiker, S.E. Pratsinis, D. Reichardt, F. Maspero, F. Krumeich, D. Günther, Fluoro-apatite and calcium phosphate nanoparticles by flame synthesis, Chemistry of Materials 17(1) (2005) 36-42.

[17] M. Bohner, T.J. Brunner, N. Doebelin, R. Tang, W.J. Stark, Effect of thermal treatments on the reactivity of nanosized tricalcium phosphate powders, Journal of Materials Chemistry 18(37) (2008) 4460-4467.

[18] J.C. Heughebaert, Contribution à l'étude de l'évolution des othophosphates de calcium précipités amorphes en orthophosphates apatitiques, Institut National Polytechnique de Toulouse, Toulouse, France, 1977.

[19] P. Scherrer, Estimation of the size and internal structure of colloidal particles by means of röntgen, Nachr. Ges. Wiss. Göttingen 2 (1918) 96-100.

[20] A. Stokes, A. Wilson, The diffraction of X rays by distorted crystal aggregates-I, Proceedings of the Physical Society 56(3) (1944) 174.

[21] J. Heughebaert, G. Montel, Preparation de l'orthophosphate tricalcique pur, Bull Soc chim Fr 89 (1970) 2923-2934.

[22] R. Van Santen, The Ostwald step rule, The Journal of Physical Chemistry 88(24) (1984) 5768-5769.

[23] M. Yashima, Y. Kawaike, M. Tanaka, Determination of Precise Unit-Cell Parameters of the α-Tricalcium Phosphate $Ca_3(PO_4)_2$ Through High-Resolution Synchrotron Powder Diffraction, Journal of the American Ceramic Society 90(1) (2007) 272-274.
[24] J. Kolmas, A. Kaflak, A. Zima, A. Ślósarczyk, Alpha-tricalcium phosphate synthesized by two different routes: Structural and spectroscopic characterization, Ceramics International 41(4) (2015) 5727-5733.
[25] C. Camiré, U. Gbureck, W. Hirsiger, M. Bohner, Correlating crystallinity and reactivity in an α-tricalcium phosphate, Biomaterials 26(16) (2005) 2787-2794.
[26] K. Hurle, J. Neubauer, M. Bohner, N. Doebelin, F. Goetz-Neunhoeffer, Calorimetry investigations of milled α-tricalcium phosphate (α-TCP) powders to determine the formation enthalpies of α-TCP and X-ray amorphous tricalcium phosphate, Acta Biomaterialia 23 (2015) 338-346.
[27] A. Mackay, A preliminary examination of the structure of α-$Ca_3(PO_4)_2$, Acta Crystallographica 6(8-9) (1953) 743-744.
[28] M. Yashima, A. Sakai, High-temperature neutron powder diffraction study of the structural phase transition between α and α' phases in tricalcium phosphate $Ca_3(PO_4)_2$, Chemical Physics Letters 372(5-6) (2003) 779-783.
[29] T. Nakano, Y. Umakoshi, A. Tokumura, Variation in crystallinity of hydroxyapatite and the related calcium phosphates by mechanical grinding and subsequent heat treatment, Metallurgical and Materials Transactions A 33(3) (2002) 521-528.
[30] A. Jillavenkatesa, R. Condrate Sr, The infrared and Raman spectra of β-and α-tricalcium phosphate ($Ca_3(PO_4)_2$), Spectroscopy letters 31(8) (1998) 1619-1634.
[31] C. Rey, O. Marsan, C. Combes, C. Drouet, D. Grossin, S. Sarda, Characterization of calcium phosphates using vibrational spectroscopies, Advances in calcium phosphate biomaterials, Springer2014, pp. 229-266.
[32] I. Demnati, D. Grossin, O. Marsan, G. Bertrand, G. Collonges, C. Combes, M. Parco, I. Braceras, J. Alexis, Y. Balcaen, Suppl 1-M3: Comparison of Physical-chemical and Mechanical Properties of Chlorapatite and Hydroxyapatite Plasma Sprayed Coatings, The open biomedical engineering journal 9 (2015) 42.
[33] H. Monma, T. Kanazawa, Millennial Special Leading Papers on Ceramics in the 20th Century: the Best of JCerSJ The Hydration of α-Tricalcium Phosphate, Journal of the Ceramic Society of Japan 108(1260) (2000) S75-S80.
[34] E. Fernandez, I. Khairoun, M. Ginebra, F. Driessens, J. Planell, Comparative study of the setting reaction kinetic of several apatitic calcium phosphate bone cements, 12th International Symposium on Ceramics in Medicine, 1999, pp. 521-524.
[35] S. Sarda, E. Fernandez, J. Llorens, S. Martinez, M. Nilsson, J.A. Planell, Rheological properties of an apatitic bone cement during initial setting, J. Mater. Sci.-Mater. Med. 12(10-12) (2001) 905-909.
[36] E. Fernández, S. Sarda, M. Hamcerencu, M. Vlad, M. Gel, S. Valls, R. Torres, J. López, High-strength apatitic cement by modification with superplasticizers, Biomaterials 26(15) (2005) 2289-2296.
[37] M. Ginebra, E. Fernández, M. Boltong, O. Bermúdez, J. Planell, F. Driessens, Compliance of an apatitic calcium phosphate cement with the short-term clinical requirements in bone surgery, orthopaedics and dentistry, Clinical materials 17(2) (1994) 99-104.
[38] H. Monma, Preparation of octacalcium phosphate by the hydrolysis of α-tricalcium phosphate, Journal of Materials Science 15(10) (1980) 2428-2434.
[39] M. Bohner, A.K. Malsy, C.L. Camiré, U. Gbureck, Combining particle size distribution and isothermal calorimetry data to determine the reaction kinetics of α-tricalcium phosphate–water mixtures, Acta biomaterialia 2(3) (2006) 343-348.
[40] E.M. Burke, G.H. Nancollas, Relation of lattice ion solution composition to octacalcium phosphate dissolution kinetics, Colloids and Surfaces A: Physicochemical and Engineering Aspects 150(1-3) (1999) 151-160.
[41] M. Bohner, R. Luginbühl, C. Reber, N. Doebelin, G. Baroud, E. Conforto, A physical approach to modify the hydraulic reactivity of α-tricalcium phosphate powder, Acta biomaterialia 5(9) (2009) 3524-3535.
[42] R. Tang, G.H. Nancollas, Abnormal dissolution of octacalcium phosphate crystals at constant undersaturation, Journal of crystal growth 212(1-2) (2000) 261-269.
[43] H. Monma, S. Ueno, T. Kanazawa, Properties of hydroxyapatite prepared by the hydrolysis of tricalcium phosphate, Journal of Chemical technology and biotechnology 31(1) (1981) 15-24.

[44] H. Monma, S. Ueno, T. Kanazawa, Composition and properties of hydroxyapatite prepared by the hydration of tricalcium phosphate, Abstracts of papers of the American Chemical Society, Amer Chemical Soc 1155 16TH ST, NW, Washington, DC 20036, 1979, pp. 64-64.
[45] C.R. Campion, S.L. Ball, D.L. Clarke, K.A. Hing, Microstructure and chemistry affects apatite nucleation on calcium phosphate bone graft substitutes, Journal of Materials Science: Materials in Medicine 24(3) (2013) 597-610.
[46] S. Kotani, Y. Fujita, T. Kitsugi, T. Nakamura, T. Yamamuro, C. Ohtsuki, T. Kokubo, Bone bonding mechanism of β-tricalcium phosphate, Journal of biomedical materials research 25(10) (1991) 1303-1315.
[47] X. Wei, O. Ugurlu, M. Akinc, Hydrolysis of α-Tricalcium Phosphate in Simulated Body Fluid and Dehydration Behavior During the Drying Process, Journal of the American Ceramic Society 90(8) (2007) 2315-2321.